

Evaluation of Wave-Current Bottom Boundary Layer Models

A Thesis

Presented in Partial Fulfillment of the Requirements for
the Degree Bachelor of Science with Distinction in the
College of Engineering of The Ohio State University

By

Claire S. Nichols

* * * * *

The Ohio State University

2005

Honors Examination Committee:

Diane L. Foster, Adviser

Thomas C. Lippmann

ABSTRACT

Widespread beach erosion is threatening coastal environments making coastal engineering, especially sediment transport, a rising field of interest. An improved understanding of sediment transport will help us to combat coastal threats such as beach erosion, harbor siltation, submerged object scour, and coastal structure failure. In coastal environments sediment is transported by both currents and waves. This environment is complicated because waves and currents interact in a way that does not allow for a linear sum of their separate behaviors.

In this effort, the wave-current bottom boundary layer physics are examined with several applied engineering models and with a more sophisticated numerical model. The models are evaluated with the mean bed stress, a parameter used for the bottom dissipation calculations in circulation models, and the peak bed stress, a parameter used for quantifying sediment transport. The numerical model, Dune, used in these calculations is a quasi-three dimensional, non-hydrostatic numerical model. The model resolves the relevant dynamics of wave and current boundary layers over smooth and rough movable sand beds and includes models for the two modes of sediment transport, bed load and suspended load ((Fredsoe *et al.*, 1999)). Model calculations were performed for 7 wave periods, 20 wave velocities, 10 current velocities, and 2 wave-current angles. The calculations were compared with three models

currently used in engineering practice (Grant-Madsen (1994), Soulsby (1993), Styles-Glenn (2000)).

Predictions of the mean and peak bed stress by Dune and the three wave-current boundary layer models are generally of comparable magnitude. However, predictions of the mean bed stress by all three engineering models diverge from Dune when the wave velocity is greater than the current velocity.

An obliquely approaching current does not have a significant effect on the peak bed stress, but does affect the mean bed stress under large wave forcing. Predictions of the peak bed stress by the Grant-Madsen, and Styles-Glenn models are consistent with the Dune simulations at large wave periods, but are larger than the Dune simulations for the smaller wave periods, indicating a greater sensitivity to inertial effects produced by the waves. These results show that there exists model divergence when the unsteady wave forcing is larger than the mean forcing. This summer the models will be evaluated with field observations obtained in a large-scale wave flume.

This is dedicated to my parents, Marie and Vance.

ACKNOWLEDGMENTS

I would like to thank, first and foremost, Dr. Diane Foster, my adviser, for giving me a great opportunity. I would also like to thank my lab co-workers for being such a great support system; Doug Dusini, Kim Hatton, Gabe Smith, and Heather Smith. Lastly, I would like to thank Dr. Chris Sherwood for advising me from long-distance.

TABLE OF CONTENTS

	Page
Abstract	ii
Dedication	iv
Acknowledgments	v
Table of Contents	vi
List of Figures	viii
Chapters:	
1. Introduction	1
1.1 Motivation	1
1.2 Continental Shelf Circulation Models	2
1.3 Wave-Current Boundary Layer Models	3
1.4 Objective	6
2. Models	7
2.1 Madsen Model	7
2.2 Soulsby Model	8
2.3 Styles and Glenn Model	9
3. Dune	11
3.1 Theory	11
3.2 Spin up	13

4. Results	14
5. Conclusions	31
Bibliography	32

LIST OF FIGURES

Figure	Page
1.1 Schematic diagram of non-linear interaction of wave and current bed shear-stresses. (Soulsby, 1997)	4
1.2 Intercomparison of eight models for prediction of mean and maximum bed shear-stress due to waves plus a current.	5
4.1 Predictions of the vertically varying resultant of the mean flow for peak periods of 5 seconds (upper panels) and 10 seconds (lower panels) and mean currents of 0.05 m/s (left panels) and 0.5 m/s (right panels). The wave-current angle, ϕ_{wc} , is 0° . The colored lines represent the mean profiles for orbital wave velocities from 0.05 m/s (blue) to 1.0 m/s (red) in increments of 0.1 m/s. Predictions of the apparent bottom roughness, z_{oa} , by the M94 model are given with \blacklozenge	15
4.2 Predictions of the vertically varying resultant of the mean flow for peak periods of 5 seconds (upper panels) and 10 seconds (lower panels) and resultant free stream mean velocities of 0.05 m/s (left panels) and 0.50 m/s (right panels). The ϕ_{wc} is 45° . The colored lines represent the mean profiles for orbital wave velocities from 0.05 m/s (blue) to 1.0 m/s (red) in increments of 0.1 m/s. Predictions of the apparent bottom roughness, z_{oa} , by M94 model are given with \blacklozenge	17
4.3 Predictions of the resultant wave-current angle for an obliquely approaching mean flow of $\phi_{wc} = 45^\circ$. ϕ_{wc} represents the angle of approach between the current and wave flows. The colored lines represent the mean profiles for orbital wave velocities from 0.05 m/s (blue) to 1.0 m/s (red) in increments of 0.05 m/s.	18

4.4	The mean Shields parameter as a function of orbital wave velocity and mean current velocity for a wave period of 5 seconds (left panels) and 10 seconds (right panels). Results are shown for Dune (a-b); M94 (c-d); S97 (e-f); SG00 (g-h). The white lines in each panel show the contours of θ_{mean} as predicted by Dune. The black lines indicate the model results for each of the three wave bottom boundary layer models. The wave current angle is 0°	20
4.5	The mean Shields parameter as a function of orbital wave velocity and mean current velocity for a wave period of 5 seconds (left panels) and 10 seconds (right panels). Results are shown for Dune (a-b); M94 (c-d); S97 (e-f); SG00 (g-h). The white lines in each panel show the contours of θ_{mean} as predicted by Dune. The black lines indicate the model results for each of the three wave bottom boundary layer models. The wave current angle is 45°	21
4.6	Inter-model comparisons of the predicted mean Shields parameter by Dune (-), M94 (●), Soulsby(×), and Styles and Glenn (+) models for peak periods of 5 seconds (upper panels) and 10 seconds (lower panels), wave-current angles ϕ_{wc} of 0° (left panels) and 45° (right panels), and mean currents, U_c , of 0.10 m/s (red) and 0.50 m/s (blue).	22
4.7	Predictions of the root-mean-square horizontal velocity for peak periods of 5 seconds (upper panels) and 10 seconds (lower panels) and mean currents, U_c , of 0.05 m/s (left panels) and 0.5 m/s (right panels). M94 predictions of apparent bottom roughness, z_{oa} , and wave bottom boundary layer thickness, δ_{wbb} , are given with \blacklozenge and \blacksquare , respectively. The colored lines represent the mean profiles for orbital wave velocities from 0.05 m/s (blue) to 1.0 m/s (red) in increments of 0.05 m/s. The wave-current angle, ϕ_{wc} , is 0°	24
4.8	Predictions of the root-mean-square horizontal velocity for peak periods of 5 seconds (upper panels) and 10 seconds (lower panels) and mean currents, U_c , of 0.05 m/s (left panels) and 0.5 m/s (right panels). M94 predictions of apparent bottom roughness, z_{oa} , and wave bottom boundary layer thickness, δ_{wbb} , are given with \blacklozenge and \blacksquare . The colored lines represent the mean profiles for orbital wave velocities from 0.05 m/s (blue) to 1.0 m/s (red) in increments of 0.05 m/s. The wave-current angle, ϕ_{wc} , is 45°	26

4.9	The maximum Shields parameter as a function of orbital wave velocity and current velocity for a wave period of 5 seconds (left panels) and 10 seconds (right panels). Results are shown for Dune (a-b); M94 (c-d); S97 (e-f); SG00 (g-h). The white lines in each panel show the contours of θ_{mean} as predicted by Dune. The black lines indicate the model results for each of the three wave bottom boundary layer models. The wave current angle is 0°	27
4.10	The maximum Shields parameter as a function of orbital wave velocity and current velocity for a wave period of 5 seconds (left panels) and 10 seconds (right panels). Results are shown for Dune (a-b); M94 (c-d); S97 (e-f); SG00 (g-h). The white lines in each panel show the contours of θ_{mean} as predicted by Dune. The black lines indicate the model results for each of the three wave bottom boundary layer models. The wave current angle is 45°	28
4.11	Inter-model comparisons of the predicted maximum Shields parameter by Dune (-), M94 (●), Soulsby (×), and Styles and Glenn (+) models for peak periods of 5 seconds (upper panel) and 10 seconds (lower panels), wave-current angles, ϕ_{wc} , of 0° (left panels) and 45° (right panels), and mean currents, U_c , of 0.10 m/s (red) and 0.50 m/s (blue).	29

CHAPTER 1

INTRODUCTION

1.1 Motivation

The coast is critical to the economic well-being of the United States. One in six jobs in the U.S. is marine related and the nation's shorelines attract more tourists every year than do national parks (Dalrymple, 2001). Widespread beach erosion is threatening coastal environments making coastal engineering a rising field of interest. Sediment transport plays a vital role in many aspects of coastal engineering. It is an important consideration for the construction of economically viable harbors, coastal flood defense, loss or growth of recreational beaches, and the safety of offshore platforms and pipelines (Soulsby, 1997). An improved understanding of sediment transport is critical for the advancement of coastal engineering. Although many advances have been made in nearshore hydrodynamic models, sediment transport models have lagged behind. First, hydrodynamic processes can be modeled with well-defined governing equations, whereas the processes of micro-scale sediment suspension and transport are less well defined. Second, simplifications to the hydrodynamic equations, when embedded in numerical schemes, can be validated by a much larger body of experimental observations. Progress in nearshore sediment transport has

been limited by both a fundamental understanding of nearshore processes and the extreme difficulty in selecting a simplified condition with which to systematically benchmark model performance. It is important to understand sediment transport in order to combat coastal threats such as beach erosion, harbor siltation, submerged object scour, and coastal structure failure.

1.2 Continental Shelf Circulation Models

Not only is the coast important to U.S. economics, it is a critical area of study all over the world. During the winter of 2002-2003, there was a multi-institution concentrated investigative effort on the Adriatic Sea. The focus of the cooperative EuroSTRATAFORM experiment is to improve our ability to understand and simulate the physical processes that deliver sediment to the marine environment and generate stratigraphic signatures (Sherwood, 2004). A motivation for studying the Adriatic Sea is the shape of Holocene deposits and the separation between the sources of sediment supply and regions of long term sediment deposition (Sherwood, 2004). In this project, the Adriatic Sea circulation is predicted by Warner, *et al.* (2003) with the Regional Ocean Model System (ROMS) the Regional Ocean Model System (ROMS). ROMS is a three-dimensional, free surface, terrain following numerical model. It employs the Generic Length Scale (GLS) approach, as proposed by Umlauf and Buchard (2003), along with one of several known turbulence closure models. The GLS approach is a two-equation model; one equation for turbulence kinetic energy and a second equation for the generic turbulence length scale quantity, given by

$$\frac{\partial k}{\partial t} + U_i \frac{\partial k}{\partial x_i} = \frac{\partial}{\partial z} \left(\frac{K_M}{\sigma_k} \frac{\partial k}{\partial z} \right) + P + B - \epsilon \quad (1.1)$$

and

$$\frac{\partial \psi}{\partial t} + U_i \frac{\partial \psi}{\partial x_i} = \frac{\partial}{\partial z} \left(\frac{K_M}{\sigma_\psi} \frac{\partial \psi}{\partial z} \right) + \frac{\psi}{k} (c_1 P + c_3 B - c_2 \epsilon F_{wall}) \quad (1.2)$$

respectively, where σ is the turbulence Schmidt number, P is production by shear, B is production by buoyancy, ϵ is dissipation, and c_1 , c_2 and c_3 are coefficients selected to be consistent with von Karman's constant and with experimental observations for decaying homogeneous, isotropic turbulence (Wilcox, 1998). Many closures can be used with the GLS method, including k-kl, k- ϵ , k- ω , and the generic model (Umlauf *et al.*, 2002). Further information about the performance of each of these schemes within the GLS method can be obtained from Warner *et al.* (2003).

ROMS and other large scale circulation models have had only limited success in the prediction of sediment transport. A difficulty with using circulation models for sediment transport modeling is scaling. For the EuroSTRATAFORM project, the horizontal grid cells are about 4-km while the nearbed vertical grid cells are about 0.1-m with 20 vertical grid levels (Warner *et al.*, 2003). A lack of computer power limits the ability for most to resolve fine scale processes within large scale models. Continental shelf circulation models rely on subgrid parameters of the bottom boundary layer dynamics for estimates of energy dissipation and sediment transport. A solution to this challenge is a hierarchy of models that inform each other across a range of domains and scales (Sherwood, 2004).

1.3 Wave-Current Boundary Layer Models

In a coastal environment the transport of sediment is induced by both waves and currents. Although the effects of waves and currents, separately, are understood, their combined effects are complicated. Their combined behavior is not simply a

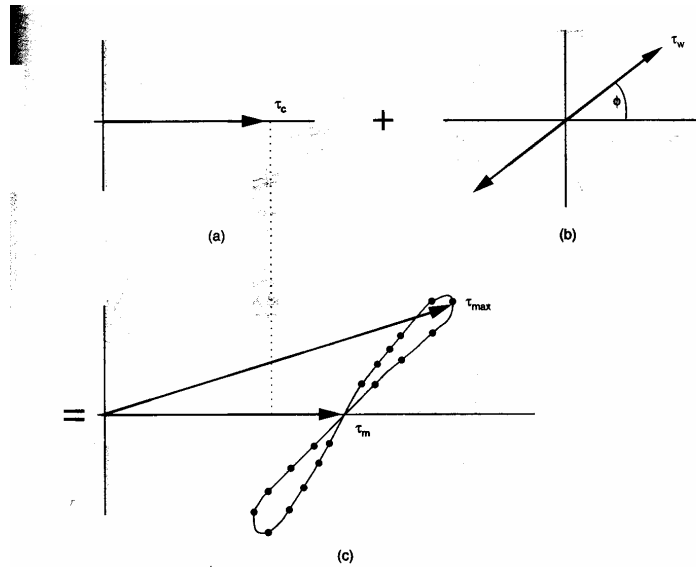


Figure 1.1: Schematic diagram of non-linear interaction of wave and current bed shear-stresses. (Soulsby, 1997)

linear sum of their separate behaviors. The non-linear interaction between the wave and current boundary layers causes the resultant bed shear-stresses to be greater than what would result from a simple addition of the wave-alone and current-alone stresses (Figure 1.1). More than 20 theories and models have been proposed to describe this theory. Eight of these theories have been compared by Richard Soulsby using their predictions of mean (τ_{mean}) and maximum (τ_{max}) bed shear-stress (Soulsby, 1997) (Figure 1.2).

Calculations of τ_{mean} are used for the parameterization of bottom dissipation, and τ_{max} for the parameterization of sediment transport. Most of the time the stresses predicted by the three models are found to differ by 30% – 40% and differences of up to a factor of 3 occur for strongly wave-dominated conditions. Soulsby performed a comparison of the 8 bottom boundary layer models to 61 laboratory values and 70

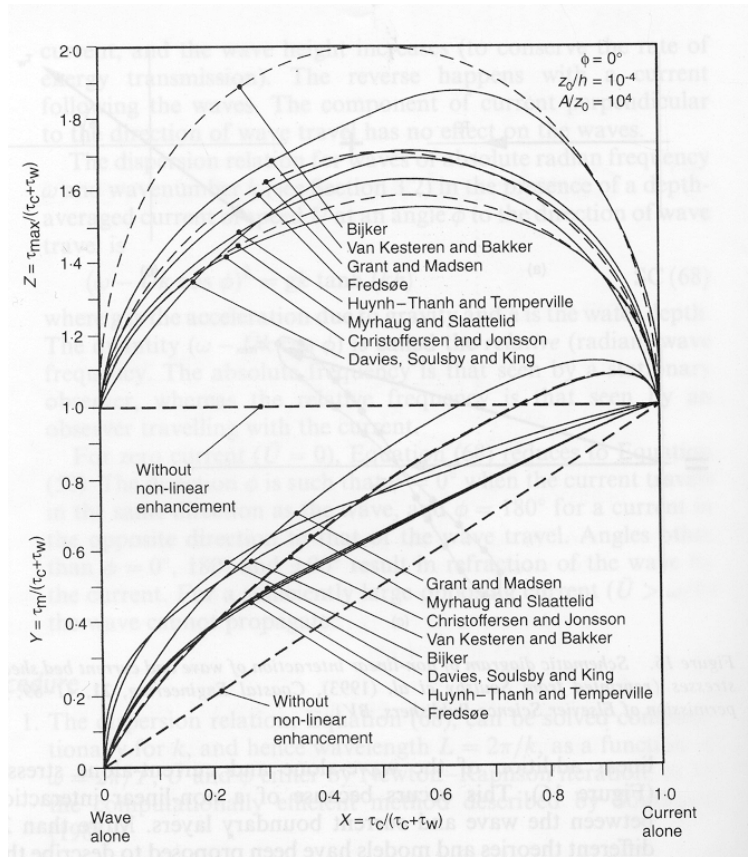


Figure 1.2: Intercomparison of eight models for prediction of mean and maximum bed shear-stress due to waves plus a current.

field values of τ_m . No one model performed the best according to all the criteria. The four models that performed the best were Grant and Madsen (1979), Fredsøe (1984), Huynh-Thanh and Temperville (1991), and Davies *et al.* (1998).

1.4 Objective

The objective of this effort is to improve our understanding of sediment transport through the study of wave-current bottom boundary layer physics. In this study a quasi-three dimensional, non-hydrostatic numerical model, Dune, is evaluated and compared to three semi-analytical engineering models using mean and peak bed shear stresses. Along with improvements in sediment transport prediction, this model assessment is designed to lead to the improvement of the hierarchy proposed by Sherwood (2004).

CHAPTER 2

MODELS

Three semi-analytical bottom boundary layer models evaluated in this investigation include Madsen (1994), Soulsby (1997), and Styles and Glenn (2000). A comparison of all four models, including Dune, is discussed in the Results section.

2.1 Madsen Model

William D. Grant and Ole Secher Madsen originally propose an analytical theory to describe the combined motion of waves and currents in the vicinity of a rough bottom and the associated boundary shear stress in 1979 (Grant and Madsen, 1979). Madsen's 1994 model, herein M94, is based on the Grant-Madsen eddy viscosity formulation. The dominating physical feature the Grant-Madsen model emphasizes is the contrasting time scales of the fluid motions. Currents are essentially steady, while surface waves are unsteady and oscillatory. As a result, the current in the region above the wave bottom boundary layer experiences a shear stress which depends not only on the physical bottom roughness, but also on the wave bottom boundary layer (Grant and Madsen, 1979). The effect of the wave bottom boundary layer on the current bottom boundary layer is parameterized with an artificial roughness which is characterizes the wave bottom boundary layer dynamics.

The governing equation for the combined wave-current environment is given by

$$\frac{\partial \mathbf{u}}{\partial t} = -\frac{1}{\rho} \frac{\partial p}{\partial x_i} + \frac{\partial}{\partial z} \left(\nu_t \frac{\partial \mathbf{u}}{\partial z} \right) \quad (2.1)$$

where t is the time variable, ρ is the fluid density, p is pressure ($p = p_c + p_w$), ν_t is the turbulent eddy viscosity, and \mathbf{u} is the velocity vector ($\mathbf{u} = \mathbf{u}_c + \mathbf{u}_w$). In M94, the eddy viscosity is parameterized with a piece-wise continuous formulation of

$$\begin{aligned} \nu_t &= \kappa u_{*r} z & \text{for } z < \delta_{wc} \\ & \kappa u_{*c} z & \text{for } z > \delta_{wc} \end{aligned} \quad (2.2)$$

where u_{*r} is the combined wave-current shear velocity and u_{*c} is the current shear velocity when inside the wave boundary layer ($z < \delta_{wc}$), and κ von Karman's coefficient ($= 0.4$). The resulting mean and maximum bed stresses are determined for a spectral decomposition of the directional wave spectrum. The matlab code for each of the three models is given in Appendix A.

2.2 Soulsby Model

The Soulsby (1997), herein S97, model is an empirical formulation. The expression for the mean bed shear stress is derived by optimizing 13 coefficients used for fitting eight different models, as mentioned in an earlier section. In comparison to the previously mentioned eight models, this approach resulted in the best fit to the data, although by definition, it can be no worse. The expression for τ_{mean} reduces to

$$\tau_{mean} = |\tau_c| \left[1 + 1.2 \left(\frac{|\tau_w|}{|\tau_c| + |\tau_w|} \right)^{3.2} \right] \quad (2.3)$$

where τ_c is the current alone bed shear-stress, given by and τ_w is the wave alone bed shear-stress. Predictions of τ_c and τ_w are given by

$$\tau_c = \rho C_D |\mathbf{u}_c|^2 \quad (2.4)$$

and

$$\tau_w = \frac{1}{2}\rho f_w |\mathbf{u}_w|^2 \quad (2.5)$$

respectively, where C_D is the drag coefficient given by

$$C_D = \left[\frac{0.40}{\ln\left(\frac{h}{z_o}\right) - 1} \right]^2 \quad (2.6)$$

\bar{U} is the steady current of depth-averaged speed, f_w is the wave friction factor, and U_w is the orbital wave velocity. Soulsby obtains the maximum bed shear stress expression using a vector addition of τ_{mean} and τ_w :

$$\tau_{max} = [(\tau_{mean} + \tau_w \cos \phi)^2 + (\tau_w \sin \phi)^2]^{\frac{1}{2}} \quad (2.7)$$

2.3 Styles and Glenn Model

The Styles-Glenn (2000), herein SG00, model is an extension of the Glenn-Grant (1987) stratified bottom boundary layer model, which adopted the GM turbulent closure scheme and modified the eddy viscosity to include a correction for suspended sediment induced stratification. First, the horizontal components of the velocity (u , v) are Reynolds averaged and separated according to their respective contributions,

$$u = u_c + u_w + u' \quad (2.8)$$

$$v = v_c + v_w + v' \quad (2.9)$$

where u_c and v_c are the current contributions, u_w and v_w are the wave contributions, and u' and v' are the turbulent velocity fluctuations. As stated, GM (1979) suggests a simple, two-layer eddy viscosity to close the fluid momentum equation. Soulsby reveals this as a weakness due to the discontinuity in the eddy viscosity at the top of the wave bottom boundary layer. To ameliorate this discontinuity, Styles and Glenn

proposes the following three-layer eddy viscosity profile,

$$\nu_t(z) = \kappa u_{*c} z \quad z_2 < z \quad (2.10)$$

$$\nu_t(z) = \kappa u_{*cw} z_1 \quad z_1 < z < z_2 \quad (2.11)$$

$$\nu_t(z) = \kappa u_{*cw} z \quad z_0 < z < z_1 \quad (2.12)$$

where z_0 is the hydrodynamic roughness, z_1 is an arbitrary scale that defines the lower boundary of the transition layer, and $z_2 = z_1 u_{*cw} / u_{*c}$, which is determined by matching the eddy viscosities at $z = z_2$. The three-layers mentioned are an inner region, the added transition region, and an outer region. The inner region is characterized by the maximum stress as a function of the wave and current contributions. The transition layer reflects the contribution to the stress by the combined flow while ensuring a decrease in turbulence transport associated with the wave. This is represented through the constant length scale z_1 , rather than the linearly increasing length scale z (Styles and Glenn, 2000). The outer region is characterized by the stress associated only with the time-averaged current. This three-layer viscosity profile was first proposed by *Glenn* [1983] and later revised by *Madsen and Wikramanayake* [1991].

The important values for this study, as aforementioned, are the bed shear stresses. The bed shear stress expressions are determined using a continuous eddy viscosity formulation. Please see Appendix A for the corresponding matlab code.

CHAPTER 3

DUNE

The numerical model used for this study is a variation of Dune2D. Dune2D was developed at the Danish Technical University for the simulation of dunes in rivers. This numerical model is now being used to resolve the relevant dynamics of wave and current bottom boundary layers over smooth and rough movable sand beds and includes multiple bed load and suspended load transport models. The model contains separate modules for the flow, sediment transport, and morphology. The morphology module is not used in this study.

3.1 Theory

The flow module of Dune solves the following quasi-3D Reynolds averaged Navier-Stokes equations,

$$\frac{\partial u}{\partial t} + u \frac{\partial u}{\partial x} + w \frac{\partial u}{\partial z} = \frac{-1}{\rho} \frac{\partial p}{\partial x} + \frac{\partial}{\partial x} \left(\nu_t \frac{\partial u}{\partial x} \right) + \frac{\partial}{\partial z} \left(\nu_t \frac{\partial u}{\partial z} \right) \quad (3.1)$$

(3.2)

$$\frac{\partial v}{\partial t} + u \frac{\partial v}{\partial x} + w \frac{\partial v}{\partial z} = \frac{-1}{\rho} \frac{\partial p}{\partial y} + \frac{\partial}{\partial x} \left(\nu_t \frac{\partial v}{\partial x} \right) + \frac{\partial}{\partial z} \left(\nu_t \frac{\partial v}{\partial z} \right) \quad (3.3)$$

(3.4)

$$\frac{\partial w}{\partial t} + u \frac{\partial w}{\partial x} + w \frac{\partial w}{\partial z} = \frac{-1}{\rho} \frac{\partial p}{\partial z} + g + \frac{\partial}{\partial x} \left(\nu_t \frac{\partial w}{\partial x} \right) + \frac{\partial}{\partial z} \left(\nu_t \frac{\partial w}{\partial z} \right) \quad (3.5)$$

where ρ represents density and ν_t is eddy viscosity. The flow is driven by a pressure gradient which is added over the entire domain at every time step (Fredsoe *et al.*, 1999). In this quasi-three dimensional version of Dune, the morphology and forcing are assumed to be uniform in the alongshore direction. The pressure gradient is artificially simulated with a combination of mean and oscillating components. The mean pressure gradient is achieved by adding a mean slope to the momentum equation. The mean flow over a single wave cycle at a given elevation is calculated and the mean slope is adjusted until the mean free stream velocity is within an acceptable tolerance to the desired flow (Nattoo, 2003). The wave pressure gradient is defined with linear wave theory (Dean and Dalrymple, 2002).

Dune can implement several turbulence closure schemes, including the $k-\epsilon$ model, the Reynolds stress model, and the $k-\omega$ model. According to Wilcox [1998] and Andersen [1999], the $k-\omega$ model has proven to perform better in regions of adverse pressure gradients. For this study, the $k-\omega$ model was employed, using the following equation,

$$\nu_t = \kappa/\omega \tag{3.6}$$

In the sediment transport module, the generated flow field is used to predict the sediment suspension with the advection diffusion equation.

$$\frac{Dc}{Dt} = w_s \frac{\partial c}{\partial y} + \nabla(\epsilon_s \nabla c) \tag{3.7}$$

where c is the concentration variable, w_s is the fall velocity, and ϵ_s is the sediment diffusivity.

The most important quantity used to determine sediment transport is the shear bed stress, τ . The Shields parameter, θ , is often used to make model comparisons

and is proportional to τ as it is found with the following equation,

$$\theta = \frac{\tau}{(\rho_s - \rho)gd_{50}} \quad (3.8)$$

The Shields parameter is used to directly find the bed load and indirectly solve for the amount of suspension through the boundary condition at the bed (Andersen, 1999). In this study models will be compared using both τ and its non-dimensional form, θ . In the Dune simulations θ_{mean} represents the magnitude of the average bed stress over a single wave period. θ_{max} is the magnitude of the peak bed stress over a single wave period. In these calculations a flat rough sand bed has been assumed. The flow is resolved with 30 vertical and 3 horizontal grid points.

3.2 Spin up

Model calculations are performed for a single sinusoidal wave over an initial fine time step of 10,000 measurements per wave to ensure model stability. Following successful initialization, calculations are performed for a set of ten sinusoidal waves over a coarser time step of 1,000 measurements per wave. Next, calculations are performed for a combined wave and current over a time step of 100 measurements per wave. Finally, the combined wave and current flow is calculated.

CHAPTER 4

RESULTS

Model simulations were performed for 7 periods ($4 \text{ sec} < T < 10 \text{ sec}$), 20 wave velocities ($0.05 \text{ m/s} < U_o < 1.0 \text{ m/s}$), 10 current velocities ($0.05 \text{ m/s} < U_c < 0.5 \text{ m/s}$) and 2 wave-current angles ($\phi_{wc} = 0$ and 45°). Following model spin up, the mean and root-mean-square horizontal velocities in both the x and y directions are calculated at every vertical cell.

Figure 4.1 shows the resultant of the predicted mean flow for two peak periods and two resultant mean currents at a wave-current angle of 0° . Each of the four cases reveals an increasing sensitivity of the mean velocity profile to increasing wave velocities. Predictions of the apparent roughness, z_{oa} , by M94 are given by,

$$z_{oa} = \exp\left(\ln\delta_{wbb}l - \frac{u_{*c}}{u_{*wc}} \ln\frac{\delta_{wbb}l}{z_o}\right), \quad (4.1)$$

where $\delta_{wbb}l$ is the wave bottom boundary layer thickness (discussed later in this section), u_{*c} is the wave-current combined friction velocity, u_{*c} is the current friction velocity and z_o is the bottom roughness ($\frac{2d_{50}}{30}$). A well defined log layer is present when the mean flow is large and wave forcing is small. However, it is more difficult to identify with small mean currents. With an increased peak period, the mean flow decreases marginally. There is also less sensitivity to the wave bottom boundary layer,

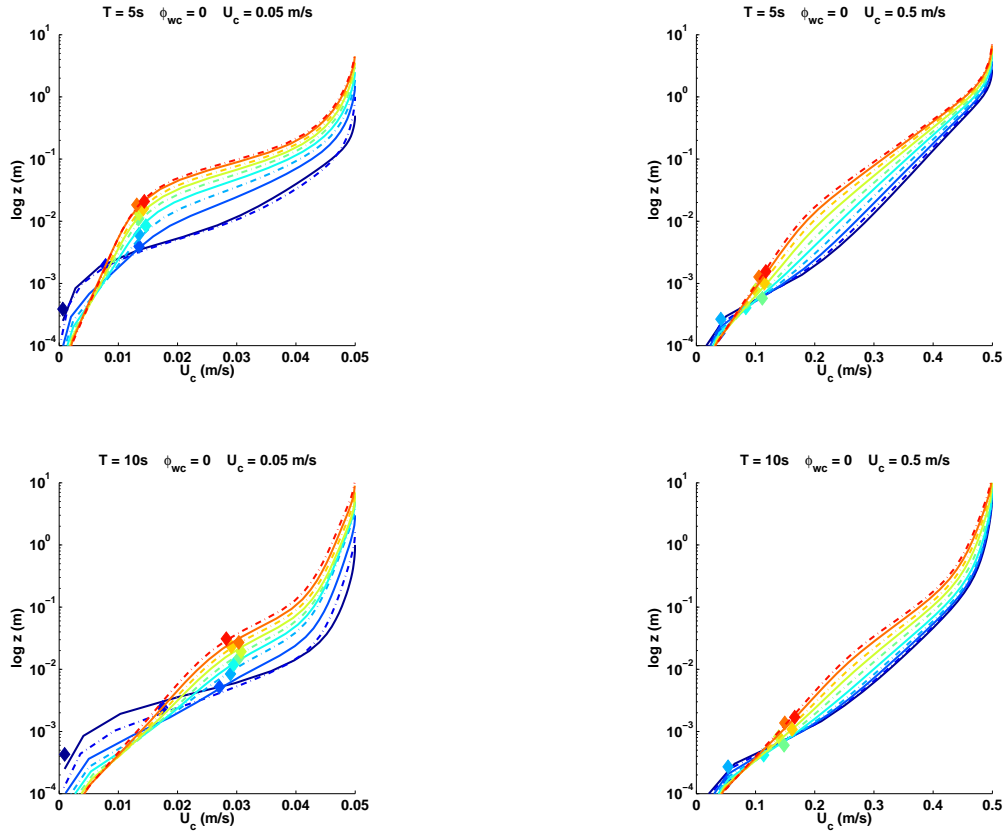


Figure 4.1: Predictions of the vertically varying resultant of the mean flow for peak periods of 5 seconds (upper panels) and 10 seconds (lower panels) and mean currents of 0.05 m/s (left panels) and 0.5 m/s (right panels). The wave-current angle, ϕ_{wc} , is 0° . The colored lines represent the mean profiles for orbital wave velocities from 0.05 m/s (blue) to 1.0 m/s (red) in increments of 0.1 m/s. Predictions of the apparent bottom roughness, z_{0a} , by the M94 model are given with \blacklozenge .

as there is less variation between the extreme wave velocities. The z_{oa} predictions by M94 show negligible variation with an increased peak period.

Figure 4.2 shows the resultant of the predicted mean flow for two peak periods and two resultant mean currents at a wave-current angle of 45° . When the mean flow obliquely approaches the wave field, the resultant mean velocity shows less sensitivity to the wave bottom boundary layer. At small orbital wave velocities (blue lines on Figures 4.1 and 4.2) the mean flow shows no sensitivity to the wave-current angle. The z_{oa} predictions are slightly lower with obliquely approaching flows.

Figure 4.3 shows predictions of vertical variations in the mean angle with a free stream wave-current approach angle, ϕ_{wc} of 45° . At large mean currents the wave-current angle asymptotes to 45° at the upper boundary. However, at a mean current of 0.05 m/s with large orbital wave forcing, the model domain prohibits ϕ from reaching the anticipated 45° . All four simulations show predictions of ϕ exceeding 45° in the velocity overshoot region indicating a modification of the mean current in response to inertial effects introduced by the wave bottom boundary layer. Close to the bed the angle decreases.

Overall, the sensitivity of the mean flow to the wave bottom boundary layer decreases with both increasing peak period and the introduction of a wave-current angle. The M94 z_{oa} predictions are mildly sensitive to the change in angle and the change in period. However, at low mean current (0.05 m/s) predictions of z_{oa} are an order of magnitude larger than the predictions at large mean currents (0.5 m/s).

The mean characteristics of Dune and the three wave-current bottom boundary layer models are evaluated with mean bed stress as non-dimensionalized with the

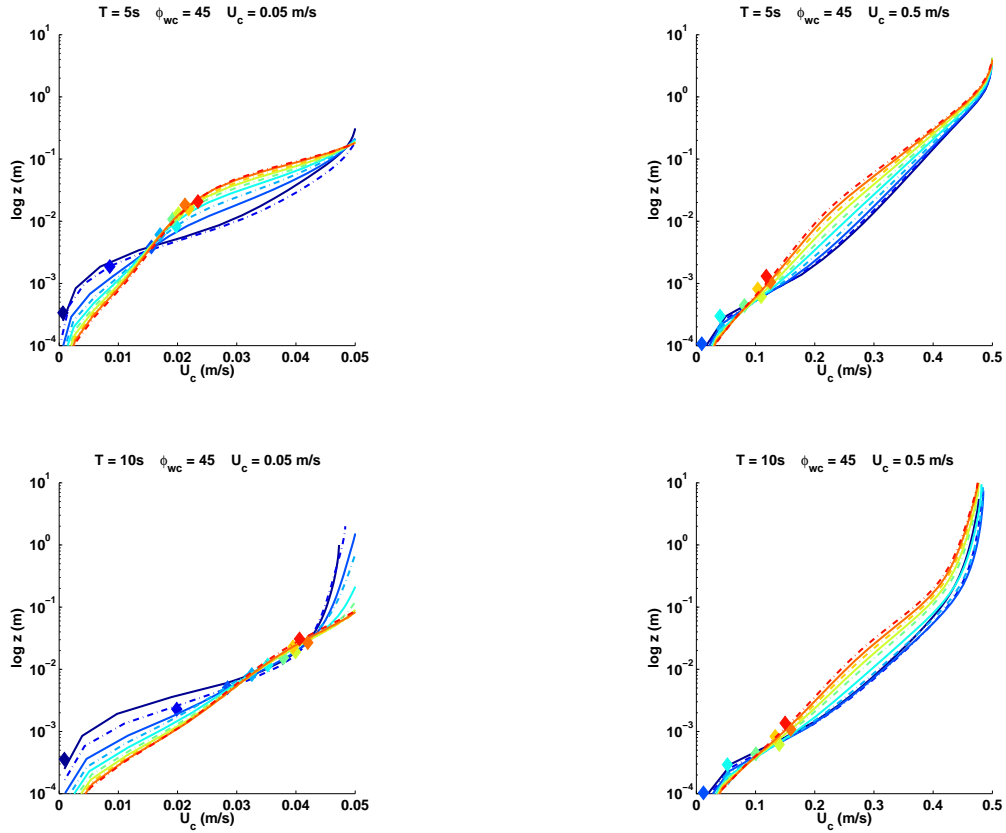


Figure 4.2: Predictions of the vertically varying resultant of the mean flow for peak periods of 5 seconds (upper panels) and 10 seconds (lower panels) and resultant free stream mean velocities of 0.05 m/s (left panels) and 0.50 m/s (right panels). The ϕ_{wc} is 45° . The colored lines represent the mean profiles for orbital wave velocities from 0.05 m/s (blue) to 1.0 m/s (red) in increments of 0.1 m/s. Predictions of the apparent bottom roughness, z_{oa} , by M94 model are given with \blacklozenge

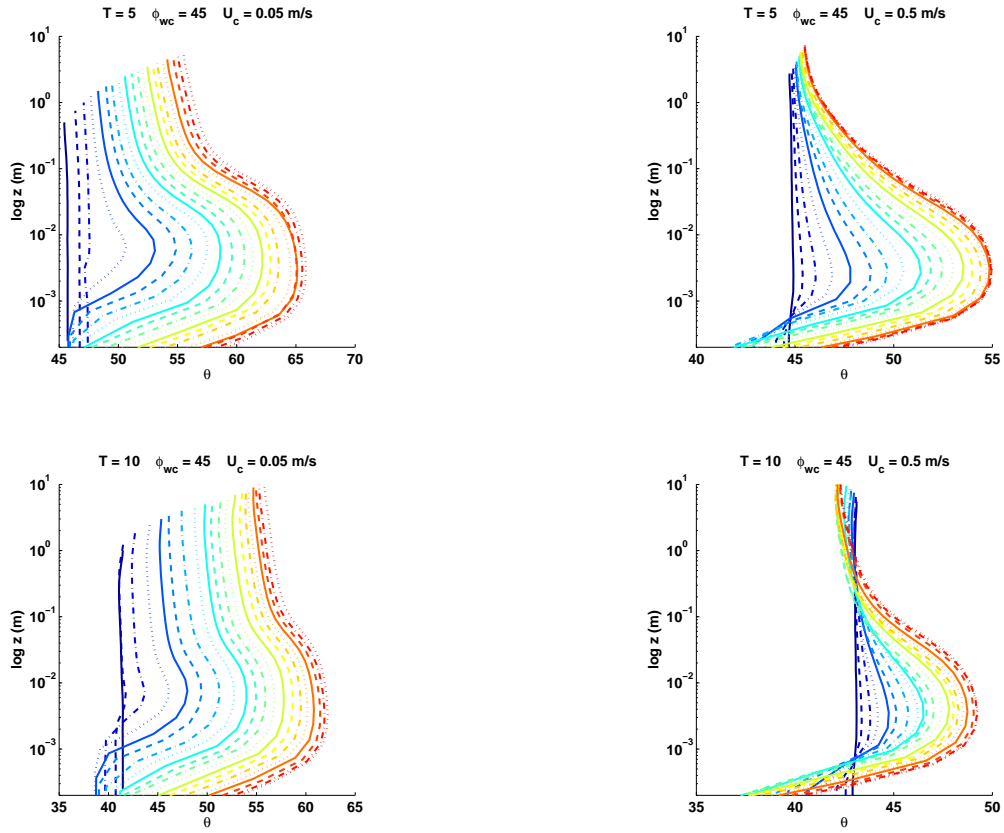


Figure 4.3: Predictions of the resultant wave-current angle for an obliquely approaching mean flow of $\phi_{wc} = 45^\circ$. ϕ_{wc} represents the angle of approach between the current and wave flows. The colored lines represent the mean profiles for orbital wave velocities from 0.05 m/s (blue) to 1.0 m/s (red) in increments of 0.05 m/s.

Shields parameter, given by

$$\theta_{mean} = \frac{\tau_{mean}}{(\rho_s - \rho)gd_{50}} \quad (4.2)$$

The mean Shields parameter, θ_{mean} , is calculated with the instantaneous bed stress over a wave period.

Figure 4.4 shows the predictions of mean bed stress over a range of wave and mean current conditions. The mean Shields parameter is also predicted with the Madsen (M94), Soulsby (S97), and Styles and Glenn (SG00) wave bottom boundary layer models. All models show an increase in θ_{mean} with increasing U_o and U_c . As the wave period increases from 5 to 10 seconds, there is a 30% to 50% increase in the mean bed stress for relatively large mean current velocities (U_c values greater than 0.3 m/s). This trend is also evident in the M94 and SG00 models. However, the S97 model is relatively insensitive to wave period. The S97 model is also relatively insensitive to orbital wave velocities greater than 0.3 m/s. The M94 and SG00 models show consistent trends with the Dune simulations. Both models are more consistent with the Dune simulations at smaller wave periods.

Figure 4.5 shows the equivalent predictions of Figure 4.4, however, using a wave-current angle of 45° . All four models show negligible sensitivity to the wave-current angle.

Figure 4.6 shows a further evaluation of the mean Shields parameter for the range of non-dimensional bed excursions defined with

$$A/kn = \frac{U_o T}{2\pi k_o} \quad (4.3)$$

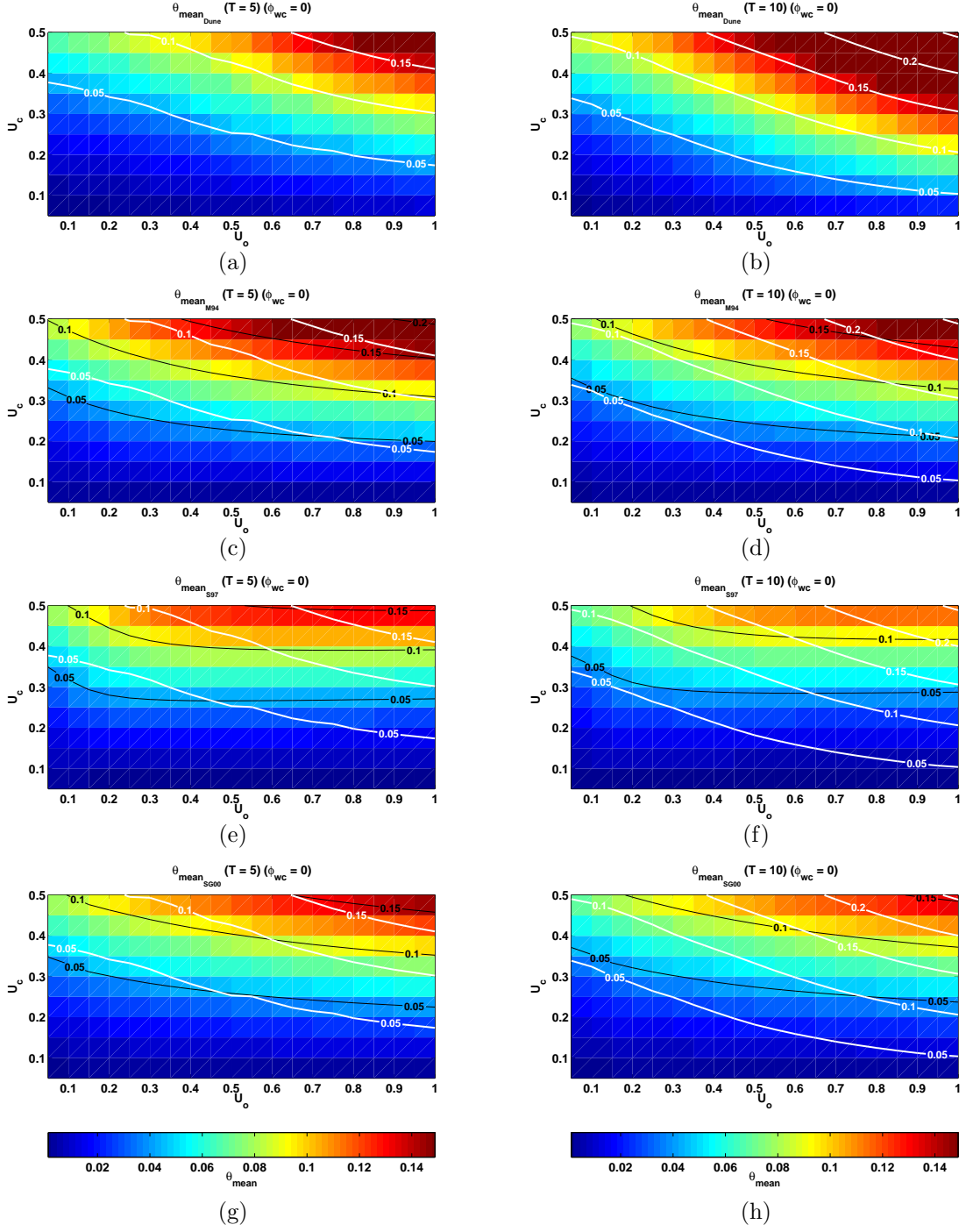


Figure 4.4: The mean Shields parameter as a function of orbital wave velocity and mean current velocity for a wave period of 5 seconds (left panels) and 10 seconds (right panels). Results are shown for Dune (a-b); M94 (c-d); S97 (e-f); SG00 (g-h). The white lines in each panel show the contours of θ_{mean} as predicted by Dune. The black lines indicate the model results for each of the three wave bottom boundary layer models. The wave current angle is 0° .

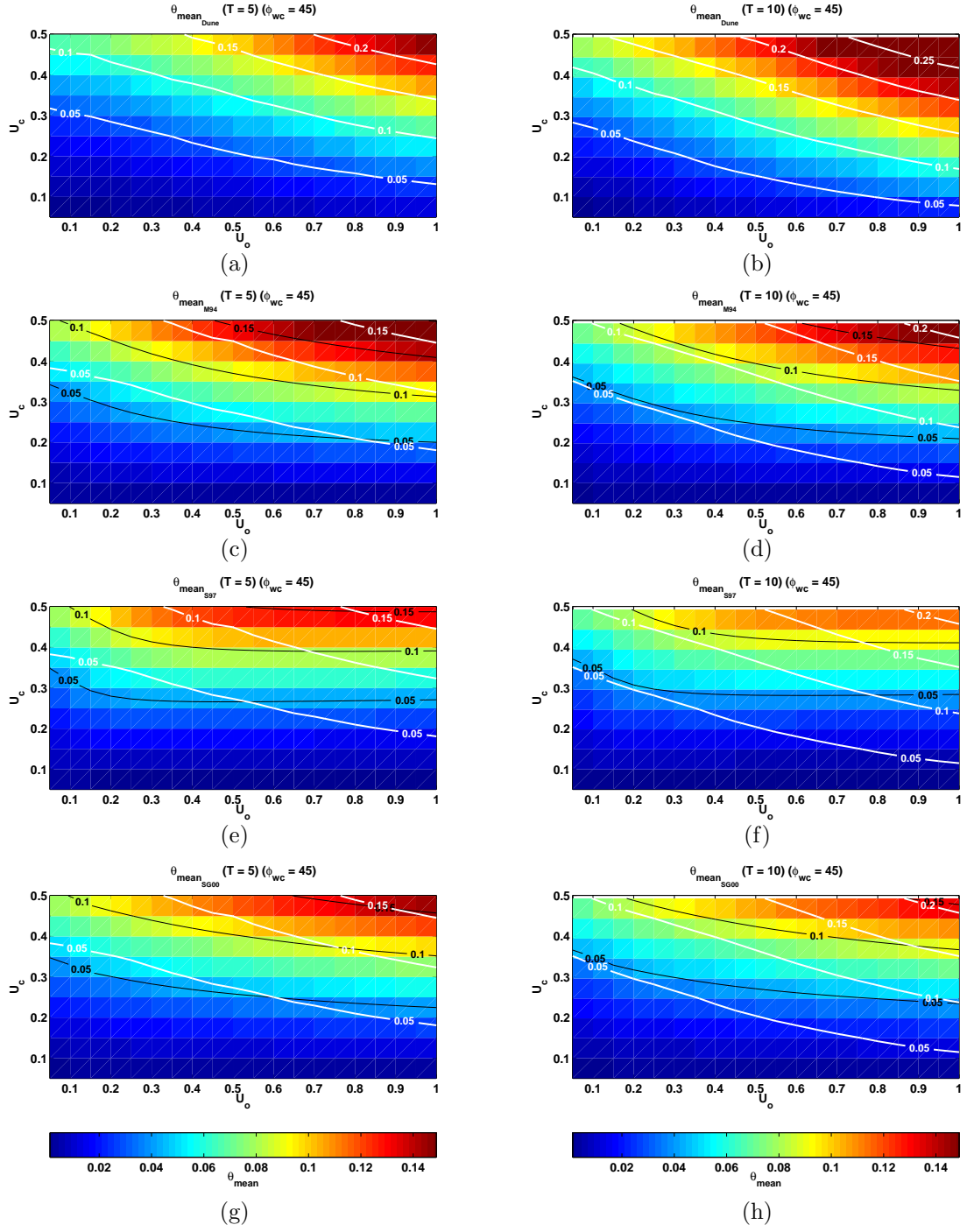


Figure 4.5: The mean Shields parameter as a function of orbital wave velocity and mean current velocity for a wave period of 5 seconds (left panels) and 10 seconds (right panels). Results are shown for Dune (a-b); M94 (c-d); S97 (e-f); SG00 (g-h). The white lines in each panel show the contours of θ_{mean} as predicted by Dune. The black lines indicate the model results for each of the three wave bottom boundary layer models. The wave current angle is 45° .

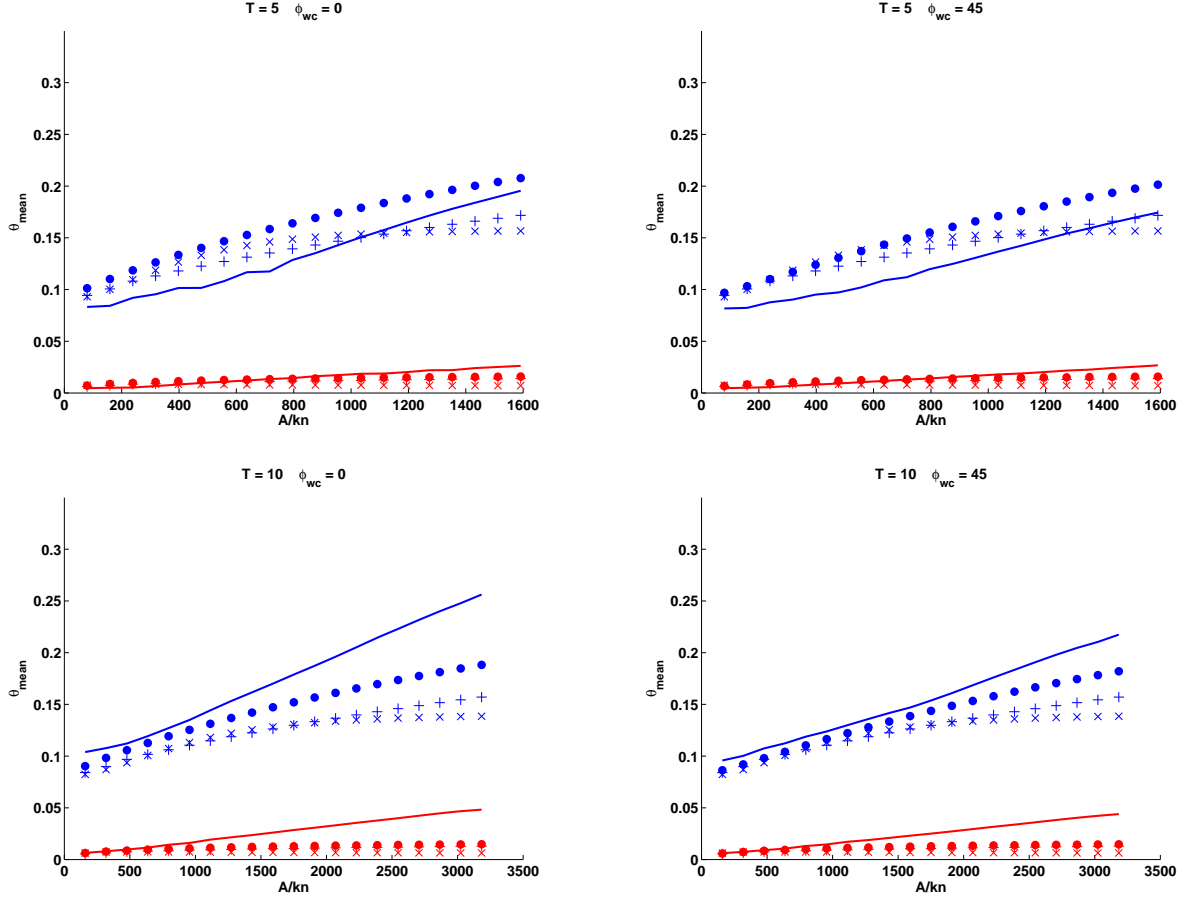


Figure 4.6: Inter-model comparisons of the predicted mean Shields parameter by Dune (–), M94 (●), Soulsby(×), and Styles and Glenn (+) models for peak periods of 5 seconds (upper panels) and 10 seconds (lower panels), wave-current angles ϕ_{wc} of 0° (left panels) and 45° (right panels), and mean currents, U_c , of 0.10 m/s (red) and 0.50 m/s (blue).

At small wave periods and small mean currents all the models predict low values of the mean Shields parameter which are not sensitive to the wave bottom boundary layer. The models diverge from the Dune predictions at the larger wave period for non-dimensional bed orbital excursions. Predictions of S97 and SG00 asymptote at orbital excursion velocities greater than 1300. Whereas, predictions by the Dune model and M94 (to a lesser extent) continue to increase.

Figure 4.7 shows the root-mean-square horizontal velocity, U_{rms} for two peak periods and two mean currents at a wave-current angle of 0° . Each of the four cases reveals an increase in free stream U_{rms} with increasing wave velocities. The Dune overshoot region increases with increasing orbital wave velocities and decreasing peak periods. Furthermore, the velocity overshoot is not effected by the change in mean current. Both M94 and Dune show an increase in wave bottom boundary layer thickness, δ_{wbb} , and the apparent bottom roughness, z_{oa} . Predictions by M94 of δ_{wbb} and z_{oa} are given by

$$\delta_{wbb} = 2 * 0.41 * \frac{U_{*wc}}{wr}, \quad (4.4)$$

and

$$z_{oa} = \exp\left(\delta_{wbb} - \frac{U_{*c}}{U_{*wc}} \log \frac{\delta_{wbb}}{z_o}\right), \quad (4.5)$$

respectively, where U_{*wc} is the wave-current combined friction velocity, wr is the angular wave frequency, U_{*c} is the current friction velocity and z_o is the bottom roughness ($\frac{2d_{50}}{30}$). The M94 predictions of the wave bottom boundary thickness, δ_{wbb} , generally occur near the zero-gradient elevation of the Dune simulations. However, Dune shows a greater sensitivity to wave periods. As expected, the M94 predictions of z_{oa} show a significant sensitivity to the mean current. For small mean currents (0.05

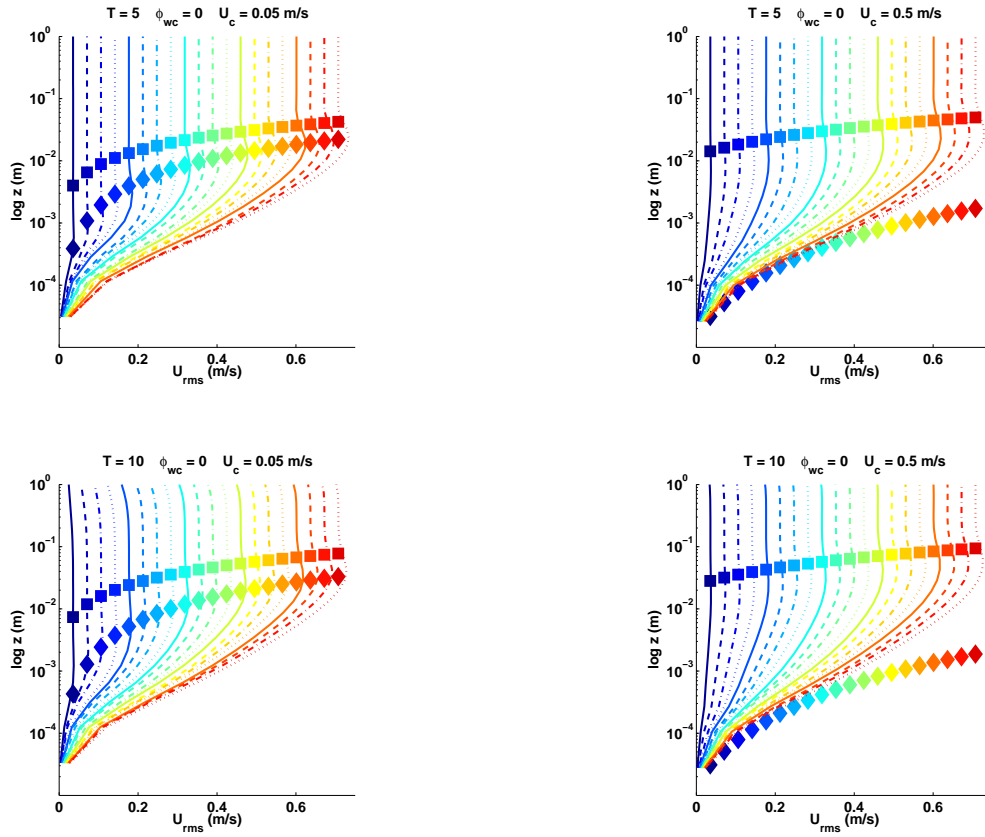


Figure 4.7: Predictions of the root-mean-square horizontal velocity for peak periods of 5 seconds (upper panels) and 10 seconds (lower panels) and mean currents, U_c , of 0.05 m/s (left panels) and 0.5 m/s (right panels). M94 predictions of apparent bottom roughness, z_{oa} , and wave bottom boundary layer thickness, δ_{wbb} , are given with \blacklozenge and \blacksquare , respectively. The colored lines represent the mean profiles for orbital wave velocities from 0.05 m/s (blue) to 1.0 m/s (red) in increments of 0.05 m/s. The wave-current angle, ϕ_{wc} , is 0° .

m/s) z_{oa} is of order the wave bottom boundary layer, but for large mean currents (0.5 m/s) the effects of the wave bottom boundary layer is small.

Figure 4.8 The results shown by 4.8 duplicate those shown by 4.7, therefore there is no effect by an obliquely approaching wave-current angle (45°) on the wave bottom boundary layer physics.

Figure 4.9 shows predictions of maximum bed stress, θ_{max} over a range of wave and mean current conditions. The maximum Shields parameter is also predicted with M94, S97 and Styles and Glenn (SG00). All models show an increase in θ_{max} with increasing U_o and U_c . As the wave period increases from 5 to 10 seconds, there is a 30% to 50% increase in the mean bed stress for relatively large orbital wave velocities (U_o values greater than 0.5 m/s). This trend is evident for all four models. M94 and SG00 show consistent trends with the Dune simulations. The two models are most consistent with Dune at higher wave periods (10 seconds) and higher current velocities (U_c greater than 0.3 m/s). With other conditions, Dune predicts a higher values of θ_{max} . S97 is most consistent with Dune at lower wave periods (5 seconds) and lower wave velocities (U_o less than 0.5 m/s).

Figure 4.10 shows the equivalent predictions of Figure 4.9, however, using a wave-current angle of 45° . All four models show negligible sensitivity to the wave-current angle.

Figure 4.11 shows a further evaluation of the mean Shields parameter for a range of non-dimensionalized bed excursion. M94 and SG00 predictions of maximum bed stress, θ_{max} , are consistent with the Dune simulations at large wave periods, but are larger than the Dune simulations for the smaller wave periods, indicating a greater

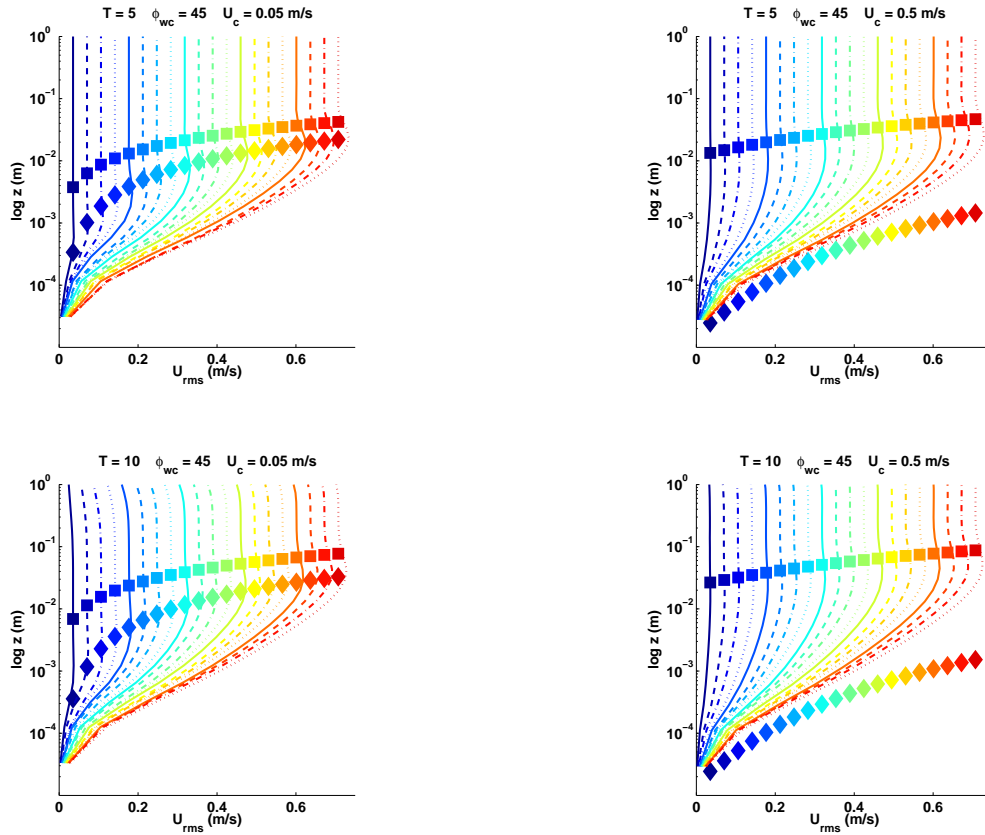


Figure 4.8: Predictions of the root-mean-square horizontal velocity for peak periods of 5 seconds (upper panels) and 10 seconds (lower panels) and mean currents, U_c , of 0.05 m/s (left panels) and 0.5 m/s (right panels). M94 predictions of apparent bottom roughness, z_{0a} , and wave bottom boundary layer thickness, δ_{wbbl} , are given with \blacklozenge and \blacksquare . The colored lines represent the mean profiles for orbital wave velocities from 0.05 m/s (blue) to 1.0 m/s (red) in increments of 0.05 m/s. The wave-current angle, ϕ_{wc} , is 45° .

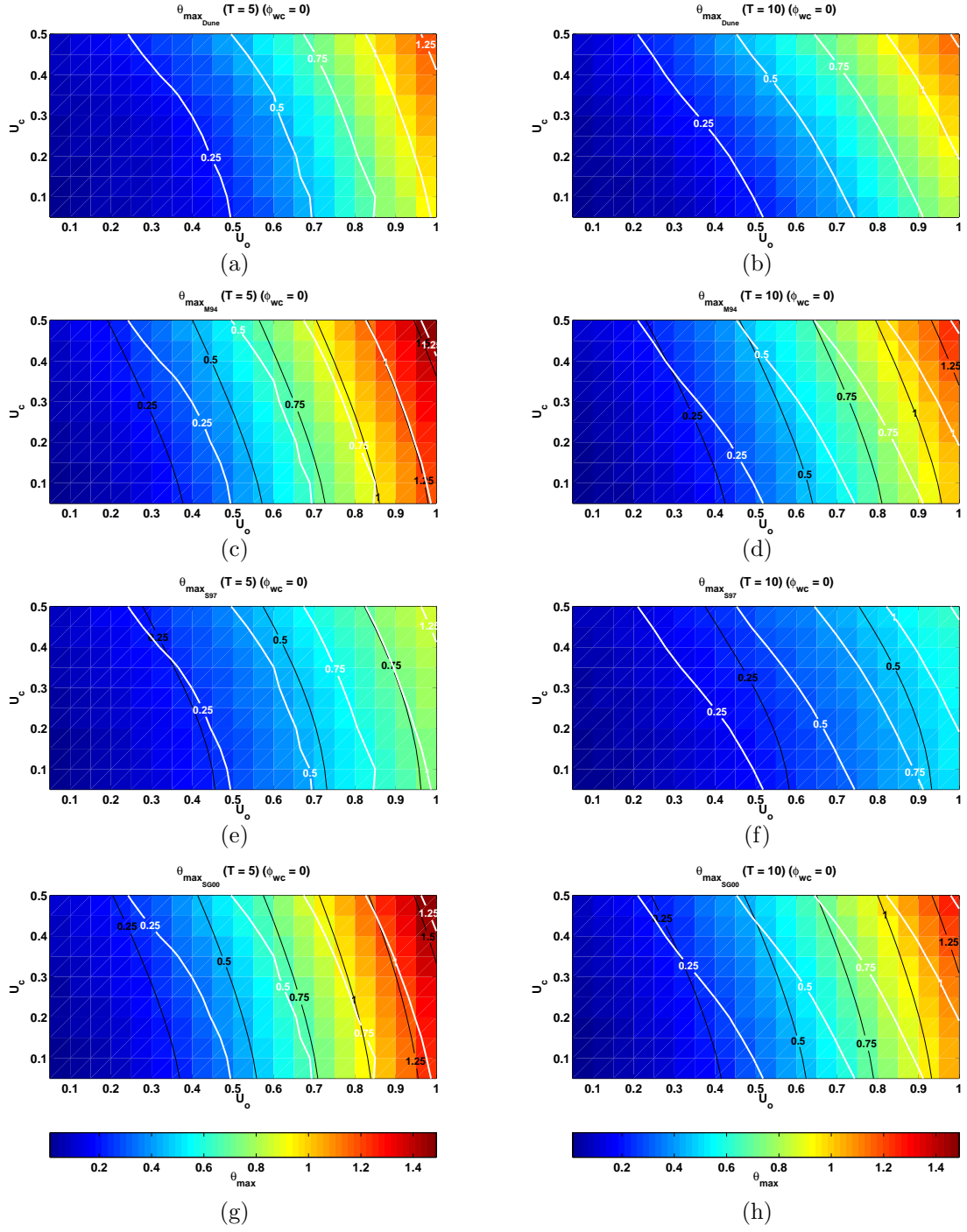


Figure 4.9: The maximum Shields parameter as a function of orbital wave velocity and current velocity for a wave period of 5 seconds (left panels) and 10 seconds (right panels). Results are shown for Dune (a-b); M94 (c-d); S97 (e-f); SG00 (g-h). The white lines in each panel show the contours of θ_{mean} as predicted by Dune. The black lines indicate the model results for each of the three wave bottom boundary layer models. The wave current angle is 0° .

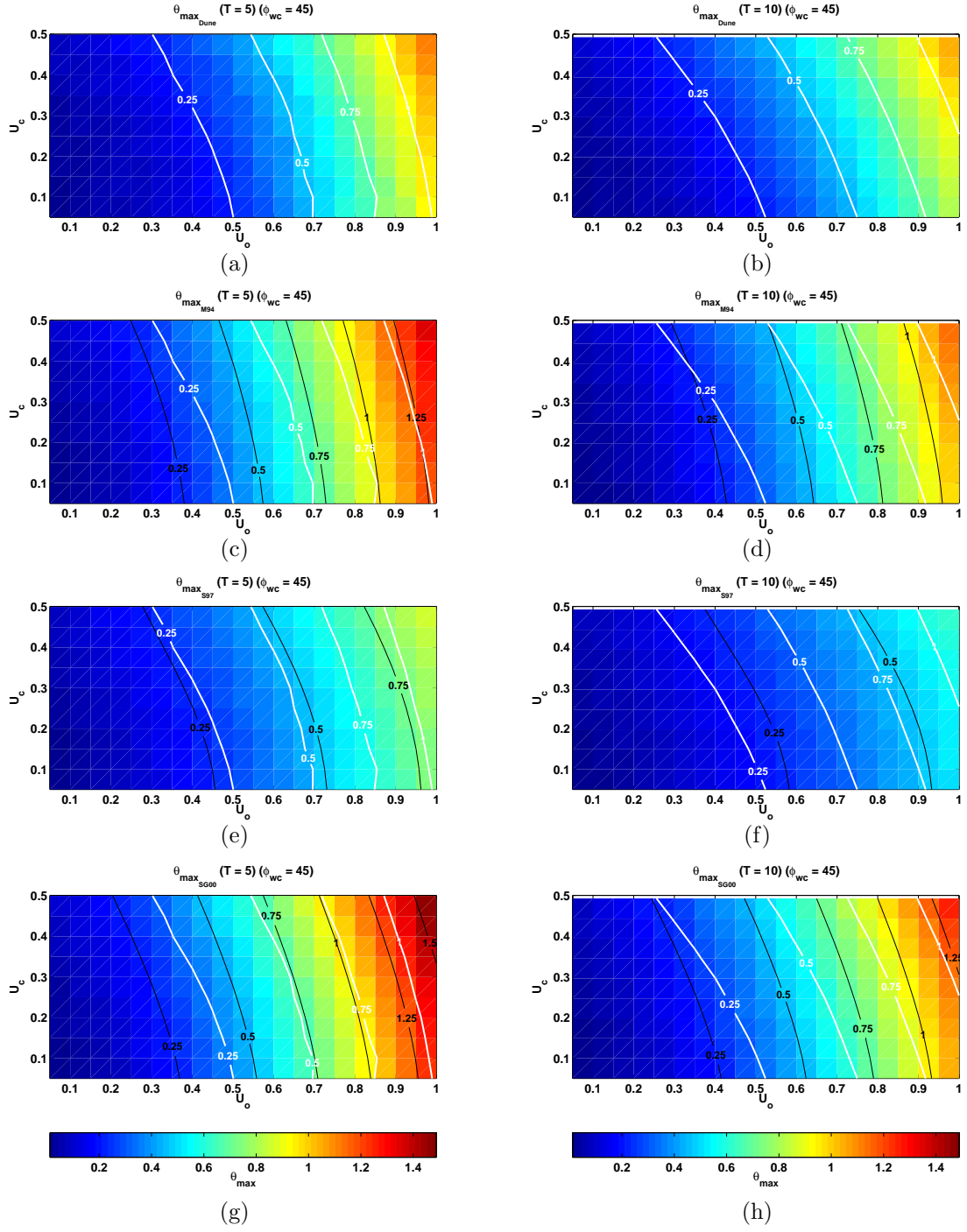


Figure 4.10: The maximum Shields parameter as a function of orbital wave velocity and current velocity for a wave period of 5 seconds (left panels) and 10 seconds (right panels). Results are shown for Dune (a-b); M94 (c-d); S97 (e-f); SG00 (g-h). The white lines in each panel show the contours of θ_{mean} as predicted by Dune. The black lines indicate the model results for each of the three wave bottom boundary layer models. The wave current angle is 45° .

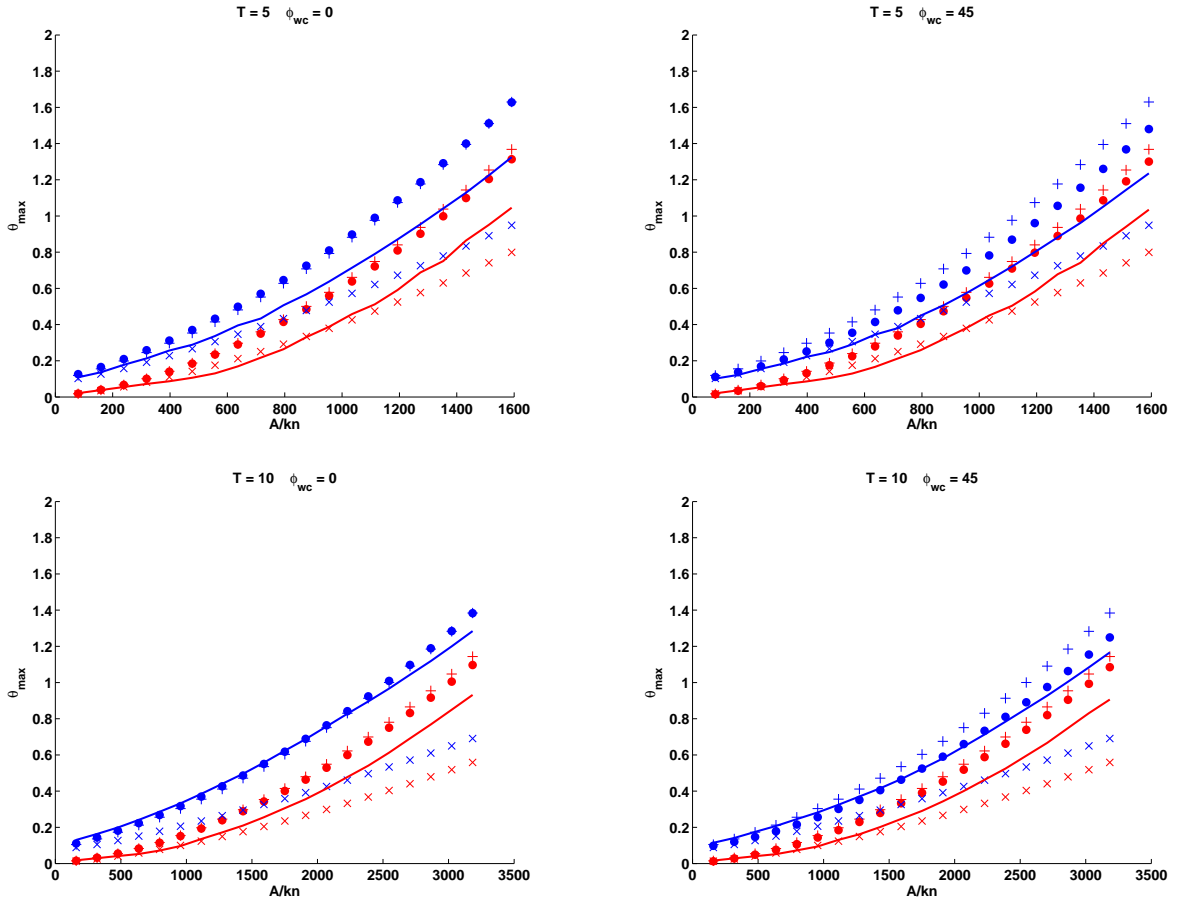


Figure 4.11: Inter-model comparisons of the predicted maximum Shields parameter by Dune (–), M94 (●), Soulsby (×), and Styles and Glenn (+) models for peak periods of 5 seconds (upper panel) and 10 seconds (lower panels), wave-current angles, ϕ_{wc} , of 0° (left panels) and 45° (right panels), and mean currents, U_c , of 0.10 m/s (red) and 0.50 m/s (blue).

sensitivity to inertial effects produced by the waves. In all cases, the Soulsby model predicts a significantly lower maximum bed stress.

CHAPTER 5

CONCLUSIONS

Model simulations of combined flow bottom boundary layers have been performed with a quasi-three dimensional bottom boundary layer model, Dune, for a range of wave and mean forcing conditions. Model performance has been examined for both the non-dimensional mean and peak bed stresses and compared against three wave-current bottom boundary layer models.

Predictions of the mean and maximum bed stress by Dune and the more simple bottom boundary layer models are generally of comparable magnitude. However, predictions of the mean bed stress by all three bottom boundary layer models diverge from Dune when U_o is greater than U_c . While an obliquely approaching current does not have a significant effect on the peak bed stress, the effect is more pronounced on the mean bed stress under large wave forcing. Predictions of the maximum bed stress by M94 and SG00 are consistent with the Dune simulations at large wave periods, but are larger than the Dune simulations for the smaller wave periods, indicating a greater sensitivity to inertial effects produced by the waves. In all cases the S97 model predicts a significantly lower maximum bed stress.

These findings do not suggest a best model, but instead reveal differences and similarities for future use when comparisons will be made with data sets.

BIBLIOGRAPHY

- Andersen, K. H. (1999). *Ripples beneath surface waves and topics in shell models of turbulence*. PhD thesis, Technical University of Denmark, Department of Hydrodynamics and Water Resources (ISVA).
- Dalrymple, R. A. (2001). Shoring up coastal engineering. *Civil Engineering*.
- Dean, R. G. and Dalrymple, R. A. (2002). *Coastal Processes with Engineering Application*. Cambridge University Press.
- Fredsøe, J., Andersen, K. H., and Sumer, B. M. (1999). Wave plus current over a rippled-covered bed. *Coast. Eng.*, 38:177–221.
- Grant, W. D. and Madsen, O. (1979). Combined wave and current interaction with a rough bottom. *J. Geophys. Res.*, 84(C4):1797–1808.
- Natoo, P. (2003). *Evaluation of Near Bed Suspension in a Wave and Current Dominated Environment*. MS thesis, The Ohio State University.
- Sherwood, C. R., e. a. (2004). Sediment dynamics in the adriatic sea: Investigated with coupled models. *Oceanography*, 17(4):58–69.
- Soulsby, R. L. (1997). *Dynamics of marine sands*. Thomas Telford Services, Ltd., 1st edition.
- Styles, R. and Glenn, S. M. (2000). Modeling stratified wave and current bottom boundary layers on the continental shelf. *J. Geophys. Res.*, 105(C10):24,119–24,139.
- Umlauf, L., Burchard, H., and Hutter, K. (2002). Extending the $k-\omega$ turbulence model towards oceanic applications. *Ocean Modelling*, 5:195–218.
- Warner, J. C., Sherwood, C. R., Arango, H. G., and Signell, R. P. (2003). Performance of four turbulence closure models implemented using a generic length scale method. *Ocean Modeling*, 8:81–113.
- Wilcox, D. C. (1998). *Turbulence Modeling for CFD*. DCW Industries, second edition.